SECURITY INSPECTION IMAGE PROCESSING METHODS APPLYING WAVELET TRANSFORM FILTERS ON TERAHERTZ ACTIVE IMAGES

INSPECCIÓN DE SEGURIDAD MÉTODOS DE PROCESAMIENTO DE IMÁGENES APLICACIÓN DE FILTROS DE TRANSFORMACIÓN WAVELET EN IMÁGENES ACTIVAS DE TERAHERTZ

Samuel Danso [1]*; Shang Liping [1]; Deng Hu [1]; Justice Odoom[1]; Liu Quancheng[1]; Mmer Mushtag[1].

1. South West University of Science and Technology-Mianyang –Sichuan, China

*Corresponding author: Samuel Danso, email: skdanso1@gmail.com

ABSTRACT

Clarity of Terahertz image is essential at various security checkpoints to avoid life's dangers and treats. However, Terahertz images are distorted by noise. Noise is frequently present in digital images during the image collection, coding, delivery, and processing phases. It is extremely difficult to remove noise from digital images without prior knowledge of the noise model. Wavelet transforms have gained popularity as a tool for image denoising. In this paper, we advance a solution to this challenge using Global Threshold selection as well as wavelet transform filters. When compared to denoising Gaussian noise at the same percentage induced, biorthogonal is the most effective denoising filter for salt and pepper noise. As the salt and pepper noise increases from 20% to 60%, the hidden security image as our target varnishes or is overpowered by the induced salt and pepper noise. We discover that despite the fact that the bior 4.4 and sym4.0 wavelet transform filters prove powerful in denoising the image, it is still not clearer and that when an image is tainted by Gaussian noise, wavelet shrinkage denoising is nearly perfect in both bior4.4 and sym 4.0, whereas when the image is tainted by salt & pepper noise, wavelet shrinkage denoising is nearly perfect in both bior4.4 and sym 4.0.

Keywords: Terahertz image; wavelet transform; biorthogonal; Gaussian noise; salt & pepper noise.

RESUMEN

La claridad de la imagen de Terahercios es esencial en varios puntos de control de seguridad para evitar peligros y golosinas de la vida. Sin embargo, el ruido distorsiona las imágenes de terahercios. El ruido está presente con frecuencia en las imágenes digitales durante las fases de recopilación, codificación, entrega y procesamiento de imágenes. Es extremadamente difícil eliminar el ruido de las imágenes digitales sin un conocimiento previo del modelo de ruido. Las transformaciones wavelet han ganado popularidad como herramienta para eliminar ruido de imágenes. En este artículo, presentamos una solución a este desafío utilizando la selección de Umbral global, así como filtros de transformación de ondas. En comparación con la eliminación de ruido gaussiano en el mismo porcentaje inducido, el biortogonal es el filtro de eliminación de ruido más eficaz para el ruido de sal y pimienta. A medida que el ruido de la sal y la pimienta aumenta del 20% al 60%, la imagen de seguridad oculta como nuestro objetivo se barniza o se ve superada por el ruido inducido de la sal y la pimienta. Descubrimos que a pesar del hecho de que los filtros de transformación de ondas bior 4.4 y sym4.0 resultan poderosos para eliminar el ruido de la imagen, todavía no es más claro y que cuando una imagen está contaminada por ruido gaussiano, la eliminación de ruido por contracción de las ondas es casi perfecta en ambos bior4.4 y sym 4.0, mientras que cuando la imagen está contaminada por ruido de sal y pimienta, la eliminación de ruido por contracción de ondas es casi perfecta tanto en bior4.4 como en sym 4.0.

Palabras clave: Imagen de terahercios; transformada wavelet; biortogonal; Ruido gaussiano; ruido de sal y pimiento.

INTRODUCTION

Image Enhancement vs. Image Denoising

Image enhancement is not the same as image denoising. Image enhancement is an objective process, while image denoising is a subjective process, as Woods and Gonzalez (2021) demonstrate. Picture denoising is a restoration technique in which an image that has been degraded is attempted to be recovered using previous knowledge of the degradation process. Image enhancement, on the other hand, is the process of altering an image's characteristics to make it more appealing to the human eye.

Terahertz images produced by the IMPATT Diode (IMPact ionization Transit Time, 2020), power, and the detector camera reflect, diffract, and scatter singles as normal image digital camera for photography do as described in chapter 3 earlier. These low-resolution images produced by the terahertz machine as shown in Fig.1 above are affected by noise and sometimes can lead to false detection at security checkpoints. Terahertz linear scanned camera operates like a normal CCD camera (Šesták et al., 2019) .

Terahertz image scanner cameras work like other forms of digital cameras. The operations of these digital cameras depict the same block diagram ideas of the terahertz capturing system. The light from regions of interest is focused onto a sensor by a lens. Color and light intensity is measured by the sensor (Yang et al., 2017).

The picture is converted to a digital signal by an analog-to-digital converter (ADC). An image-processing block improves the image and compensates for some of the other camera blocks' shortcomings. The image will be stored in memory, and a monitor will be used to preview it. Some blocks are there to give the user power. The lens, sensor, and ADC, as well as the image

processing block itself, add noise to the image.

Millions of tiny light-sensitive components make up the sensor (Jang & Hwang, 2020). They have different physical, electrical, and optical properties, which introduces signal-independent noise (dark current shot noise) into the acquired image. The photon shot noise is another form of shot noise. This happens because the amount of photons detected varies depending on which part of the sensor you're looking at. Amplification noise, which is Gaussian in nature, is introduced when sensor signals are amplified. In the digitization step, the ADC introduces thermal and quantization noise. Part of the noise is amplified by the image-processing block, which also introduces its own rounding noise. Since there are only a finite number of bits to reflect intermediate floating point results during computations, rounding noise occurs (Terasense, 2020).

Since it is symmetric, continuous, and has a smooth density distribution, most denoising algorithms assume zero mean additive white Gaussian noise (AWGN).

In reality, however, several other forms of noise exist. One example is correlated noise with a Gaussian distribution (Gonzalez-Lee et al., 2021). Poisson, Laplacian, and non-additive Salt-and-Pepper noise are examples of various noise distributions. Bit errors in image transmission and retrieval, as well as in analog-to-digital converters, cause salt-and-pepper noise. A scratch in a photograph is another example of noise. Signal-dependent or signal-independent noise exists. For instance, consider the quantization procedure (Liu et al., 2019) (Erçelebi, 2004) (dividing a continuous signal into discrete levels)

However, a lock-in-amplifier cannot be synchronized to multiple pixels resulting in a significant reduction in SNR as compared to the scanned approach (Wanget al., 2019). Finally, scattering is a concern for THz systems.

Scattering is a common issue that many imaging modalities face. The scattering of X-ray photons induces artifacts in reconstructed images and is the dominant transport phenomenon in optical tomography. The photon propagation is modeled using a diffusive method in optical tomography reconstruction algorithms. Because of their longer wavelength, THz photons undergo less Rayleigh scattering than optical and X-ray photons. Scattering, on the other hand, is still a problem in T-ray imaging, and accurately modeling the scattering process could support future imaging algorithms.

The most challenging aspect of using region-based methods is figuring out how to create acceptable similarity standards for region-based methods. In the application of denoising in imaging techniques, various forms of filters are used.

By forming an exponentially formed filter kernel, the Frost Filter (Frost et al., 1982) achieves a balance between averaging and an all-pass filter. The filter's answer varies locally according to the coefficient of variation likewise wavelet transforms filters.

THE GENERAL NOISE ISSUES IN TERAHERTZ IMAGES

Another challenge faced by THz imaging systems is the signal-to-noise ratio. This is inherently tied to the average power of the THz emitter. In THz time-domain spectroscopy systems, a very high SNR can be achieved. However, in imaging applications, several factors combine to dramatically reduce the SNR to the point where it becomes a limiting concern. Some of these factors worth pointing out include the need to accelerate the imaging acquisition speed and the high absorption of many materials. Significant advances are required in the acquisition speed of THz systems to achieve real-time imaging. Conventional THz imaging systems rely on scanning the sample in the x and z dimensions to obtain an image. This places a severe limit

on the available acquisition speed. Recently, two-dimensional (2D) electro-optic sampling has been used like a CCD camera to provide a dramatic increase in speed of imaging.

Denoising sometimes introduces noise into a picture as shown figure 1. The following are some of the disturbance artifacts caused by denoising:

1. Blur: The picture can have smooth edges due to the impedance of high spatial frequencies.
2. Ringing/Gibbs Concept: Quantization of high frequency transform coefficients can result in picture oscillations or ringing distortions.
3. Staircase Damage: Data loss of high-frequency elements in the image can result in stair-like structures.
4. Checkerboard Damage: Denoised images may have checkerboard structures on occasion.
5. Wavelet edges effects noticeable in the denoised images, these are distinct repeated wavelet-like structures that occur in wavelet domain architectures.

Figure 1: Terahertz acquisition image system and samples
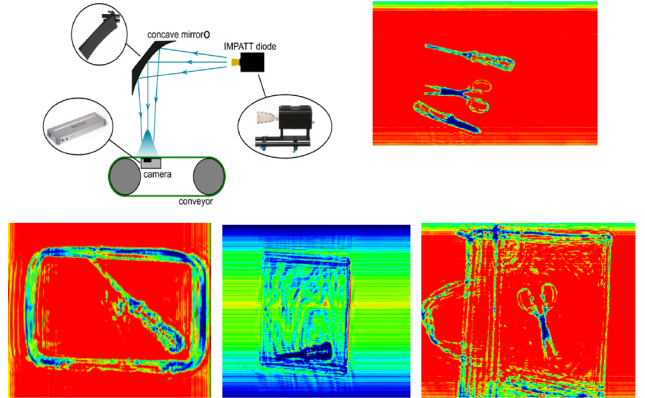
Several applications are used for image and signal processing.

WAVELETS IN IMAGE APPLICATIONS

There are serval wavelet operators (Mishra et al., 2017) (Cheng et al., 2015) (Laine, 2000) (Zhong, and Ning, 2000) (Starck et al., 2010) (Jiang, 2008) (Howlader & Chaubey 2010) used for image processing either dimensional or multi-dimensional image filtering properties applied to orthogonal and biorthogonal filters as shown in table 1.

In this section, the most commonly used for image denoising and enhancement images.

Table 1. Wavelet properties base on their families and their functions.

Wavelets with Filters			Wavelets without Filters	
With compact support		With non-compact support	Real	Complex
Orthogonal	Biorthogonal	Orthogonal		
Db, haar, sym, colf	bior	Meyr, dmey, btlm	gous, mexh, morl	cgou,shan,fbsp, cmor

Wavelet for denoising

An orthogonal wavelet such as Symlet or Daubechies wavelet is good for denoising signal whiles a biorthogonal wavelet can be good for image processing. Finally, the biorthogonal wavelet filter has a linear phase which is good for image reconstruction and for compression such as bior4.4 or rbior3.9 as shown in table 1.

Wavelet for Compression

Biorthogonal wavelet particularly bior4.4 or rbior 3.9 is good for image compression because they are symmetric hence linear.

Wavelet with higher vanishing moments should be considered because such wavelet produces fewer significant coefficients, therefore the majority of the coefficient are neglected to

achieve compression results. Additionally, higher vanishing moments causes more regular wavelet, therefore, smooth reconstruction of image or signal. Maximal Overlap Discrete Wavelet Transform (MODWT) is needed when the goal is geared toward acquiring variance analysis. This MODWT conserve energy for analysis stage by using orthogonal wavelet such as db, sysm.

Other Applications of Wavelet.

- Image watermarking: Wavelet with higher vanishing moments (more regular) and symmetry(linear phase) such as bior 6.8
- Edge detection: Wavelets with smaller support (less vanishing moments) such as haar, bior1.1
- Ecg signal extraction: sym4 is widely used for this purpose
- Feature extraction for OCR: Wavelet with higher vanishing moment such as db10.

Frequency filters

The image and signal processing tool for denoising and multispectral possibilities is wave-transforming (WT). In contrast to the transformation Fourier FT where only frequency signal is known, whiles WT is suitable for transitory and non-stationary signals frequency response varies in time (Robinson et al., 2010) (Baili et al., 2009). Signals are typically limited by the band, which corresponds to finite energy, which means that only a limited range of scales needs to be used. Inversely proportional to the frequency of the radius. Consequently, high-scale and dilated wavelets are the corresponding low frequencies. Global information is extracted from a signal known as approximations utilizing wavelet analysis on a high scale. While fine information is extracted from a signal core details at the low scales.

THE FOURIER TRANSFORM THEORY

Fourier transform has two forms: the Content

Time Signal and Discrete-Time Signal. Both can be mathematically expressed as equations 1 & 2 and figure 2 below.

For Fourier transform for Content Time Signal = Infinite extent

$$F(\omega) = \int_{-\infty}^{\infty} f(t)e^{-j\omega t}dt \tag{1}$$

For Fourier transform for Discrete-Time Signal = Finite extent.

$$F(\omega) = \sum_{-\infty}^{+\infty} f(n)e^{-j\omega n} \tag{2}$$

Figure 2. Signal decomposition
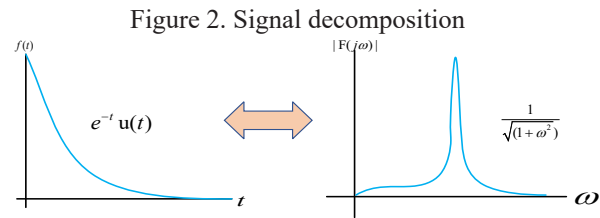
Decomposition of the signal $f(t)$ in an infinite number of sine/cosine waves (harmonics).

FT does not identify exactly where an event occurs meaning the time information is missing and only frequency and magnitude are given as shown in figure 2. This nature makes it discontinuous and bursts of signals.

The chirp signal, the content increase with time as the corresponding full spectrum, but when the signal is reversed, its frequency will be decreasing with time, then the same magnitude of full spectrum would be derived which tells what is happening in the time domain. The solution to this problem was proposed by Dennis Gabor (1946) introducing the STFT as an advantage but to analyze only a small section of the signal at a time with a technique called Windowing the Signal. This is done when the Segment of signal is assumed stationary as expressed in below eqn 3 and figure 4.

A function of time and frequency

$$STFT_x^{\omega}(t', \omega) = \int [x(t).W(t - t')].e^{-j\omega t}dt \tag{3}$$

Figure 3. STFT Signal representation

Figure 4: Morlet wavelet
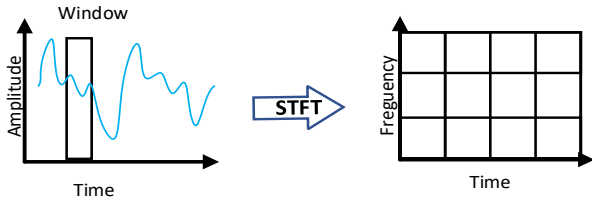
The drawback also in STFT is the Unchanged Window, which makes it uncertain because we cannot know what frequency exits at what time intervals.

The uncertainty Procedure of Resolution goes like this:

- If Narrow window (good time resolution) then a poor frequency resolution is obtained.
- If Wide window (poor time resolution) then a good frequency resolution would be the outcome.

Wavelet for Compression

A wavelet is a waveform of effectively limited duration that has an average value of zero. It is defined as,

$$\psi_{a,b}(t) = \frac{1}{\sqrt{a}} \psi\left(\frac{t-b}{a}\right) \quad a, b \in \mathbb{R} \tag{4}$$

Here a and b are called Dilation (Scale) and Translation (Position) parameters respectively.

An example wavelet is shown below. With the help of a we stretch the wavelet to size and with help of b the wavelet will be shifted a long time period. In eqn. 5 is a complex wavelet as shown as $Morlet\ Wavelet$.

$$\psi(t) = e^{j\omega_0 t} e^{-\frac{t^2}{2}} \tag{5}$$
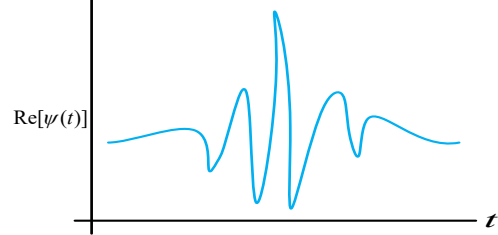
THE THEORY OF WAVELET

Comparing the Fourier transform and the wavelet transform

In Fourier transform, any signal is expressed by its harmonics component, which is of sine, cosine, and an infinite number of sine cosine. This means the main function of FT is a constituent of sinusoids of different frequencies while in Wavelet transform the signal can be expressed by wavelets of different scales and positions. The main constituent of wavelet transform is a wavelet of different scales and positions.

In this section, the theory of wavelet is advanced with emphasis on the various categories.

a. Categories of Wavelet Transforms

Wavelet transform is grouped into two. They are Continuous Wavelet Transform (CWT) and Discrete Wavelet Transform (DWT).

Figure 5. Fourier transform vs wavelet transform
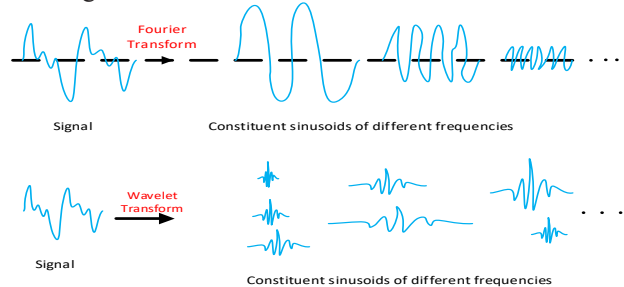
Continuous Wavelet Transform (CWT)

The Continuous Wavelet Transform (CWT) of a signal $f(t)$ is then given by the equation 6.

$$CWT(a,b) = (f, \psi_{a,b}) = \frac{1}{\sqrt{a}} \int_{-\infty}^{+\infty} f(t).\psi^*\left(\frac{t-b}{a}\right) dt \qquad (6)$$

Here, $(f, \psi_{a,b})$ is the $\mathbb{L}^2$ inner product

The results of the CWT give many wavelet coefficients, which are a function of a (scale) and b (position). Wavelet coefficients are arranged in the diagram below. For instance, the first line is all the coefficient of scale as shown in figure 6 (c11-c1n), then scale two is arrange from c21-c2n and scale three it being arranged c31-c3n until all the coefficient is arranged. With the a is compressed and wavelet is captured all high frequencies component available in the signal and with the b the wavelet is sliced along the time axis and then multiplied with signal and finally integrated. It is repeated until the entire coefficient at scale 3 is derived as shown in the diagram. At low scale fine frequency details as wavelets are compressed it captures high frequency as high scale the wavelet is stretch and it captures low frequency details.

Figure 6. Continuous wavelet transformation
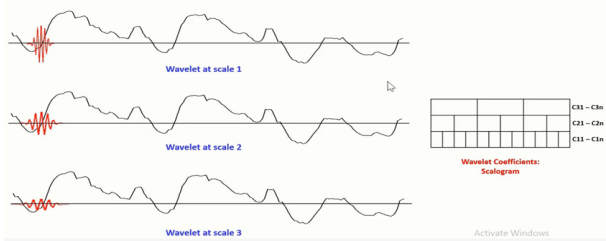
Discrete Wavelet Transform (DWT)

The constant transformation of the wavelet gives us lots of redundant data. DWT requires less space, using space-saving coding based on the fact that wavelet families are orthogonal or biorthogonal so that redundant analysis is not performed. The DWT matches its continuous version, usually sampled on a dyadic grid, meaning that the scales and translations are powerful.

The DWT is calculated in practice by a high-pass and low-pass filter to successively pass a signal. The High-Pass filter that forms the

wavelet function generates approximations A for each decomposition level. Details of D (Mallat, 1999) (Boix & Cantó, 2013) are provided by the complementary low-pass filter representing the scaling function. This algorithm is referred to as subband coding. During the filtering process, the resolution will be modified, and the sampling scale will be changed either by up or down.

The a is chosen to be an integer power of one fixed dilation parameter $a_o > 1, i.e. a = a_o^m$. The different values of m correspond to wavelets of different widths. The narrow wavelets are translated by small steps, while wider wavelets are translated by larger steps. Therefore, b is discretized by $b = nb_0 a_0^m, where\ b_0 > 0\ is\ fixed\ and\ n \in \mathbb{Z}$. The corresponding discretely labeled wavelets are, therefore,

$$\psi_{m,n}(k) = a_0^{-\frac{m}{2}} \psi\left(a_0^{-m}(k - nb_0 a_0^m)\right) m, n \in \mathbb{Z} \qquad (7)$$

For a given function $f(k)$, the inner product $(f, \psi_{m,n})$ then gives the discrete wavelet transform as given as,

$$DWT(m,n) = (f, \psi_{m,n}) = a_0^{-\frac{m}{2}} \sum_{k=-\infty}^{\infty} f(k).\psi^*(a_0^{-m}k - nb_0) \qquad (8)$$

Discrete Wavelet Transform (Multi Resolution Analysis (MRA)

If scales and positions are chosen, based on powers of two, so-called Dyadic scales and positions, their analysis becomes much more efficient and just as accurate.

S. Mallat (2009) proposed this. For some very special choice $\psi(k)$ with good time-frequency localization properties such that the,

$$\psi_{m,n}(k) = 2^{-\frac{m}{2}} \psi(2^{-m}k - n) \ m, n \in \mathbb{Z} \qquad (9)$$

constitutes an orthonormal basis for $\mathbb{L}^2(\mathbb{R})$.

For a given function $f(k)$, the inner product $(f, \psi_{m,n})$ then gives the discrete wavelet transform as given as,

$$DWT(m,n) = (f, \psi_{m,n}) = 2^{-\frac{m}{2}} \sum_{k=-\infty}^{\infty} f(k).\psi^*(2^{-m}k - n) \qquad (10)$$

The wavelet decomposition of a signal $s(t)$ based on the multi resolution theory given by S. Mallet (2009) can be done using digital FIR filters as shown in figure 7.

ORTHOGONAL AND BIORTHOGONAL WAVELET MATHEMATICS

The mathematical foundations of orthogonal and biorthogonal wavelets are examined critically in this section.

The Haar wavelet function is defined as follows:

Figure 7. Wavelet decomposition of a signal
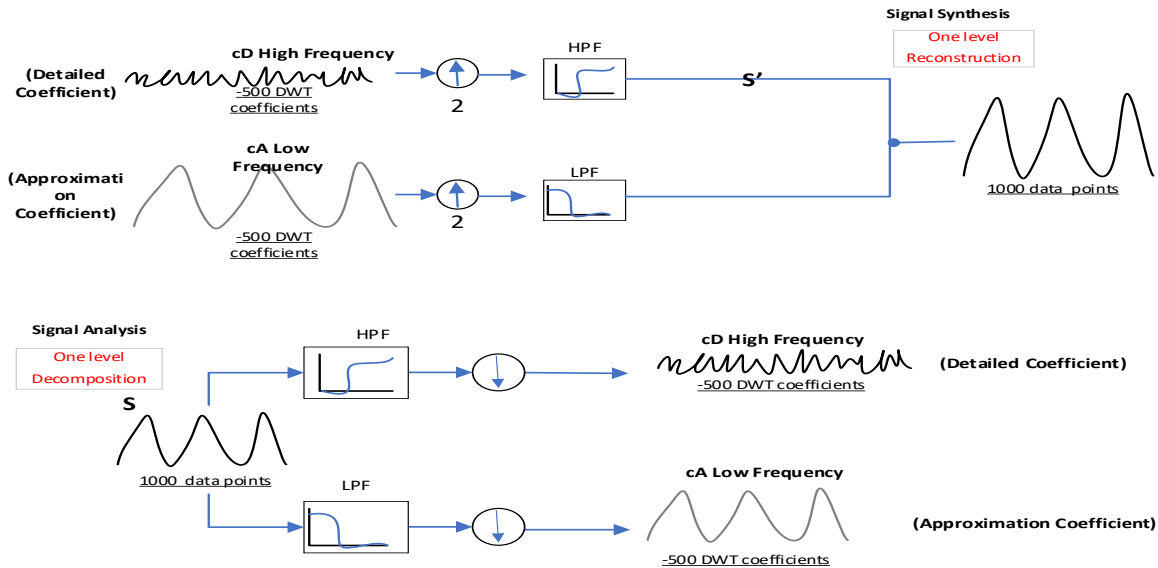
$$\psi^{Haar}(x) \begin{cases} 1, & 0 \le x \le \frac{1}{2} \\ -1, & \frac{1}{2} \le x \le 1 \\ 0, & otherwise \end{cases} \quad (11)$$

ψ^{Haar} $_{j,k}$

$$(x) = 2^{j/2}\psi^{Haar}(2^j x - k) = \begin{cases} 1, & \frac{k}{2^j} \le x \le \frac{k+1/2}{2^j}, \\ -1, & \frac{k+1/2}{2^j} \le x \le \frac{k+1}{2^j}, \\ 0, & otherwise \end{cases} \quad (12)$$

Characterizes simple wavelet scale A ϕ (t) is a scaling function in time t

$$\phi_{j,k(t)} = 2^{j/2}\phi(2^j t - k) \quad (13)$$

where j is the scaling parameter and k is the translation parameter, and both j and k are part of S. A set of integers is referred to as S.

Translation and scaling are necessary for the formation of a class of functions, and dilation can be used to form the equation 14.

$$\phi(t) = \sqrt{2 \sum_n h_n \phi(2t - n)} \quad (14)$$

The filter coefficient is specified here, and the scaling factor is. The presence of the parental wavelet (wavelet function that defines the basic wavelet shape) is denoted by

$$\psi_{j,k(t)} = 2^{j/2}\psi(2^j t - k) \quad (15)$$

$\phi(t)$, represents the weighted sum of the shifted $\phi(2t)$ this generated the orthogonal fundamental for $L^2 R$

$$\psi(t) = \sqrt{2 \sum_n g_n \phi(2t - n)} \quad (16)$$

The wavelets section necessitates the use of orthogonal complement space. The wavelet filter and scaling coefficients are required for orthogonality, and they are connected by:

$$g_n = (-1)^n h_{1-n} \quad (17)$$

A Cartesian coordinates mirror high pass and low

pass filter is what this pair of g_n and h_n is called. The biorthogonal wavelet is a consequence of this method of the classical orthogonal generalization

The dual scaling function is depicted here as follows, mathematically:

$$\tilde{\phi}(t) = \sqrt{2} \sum_n \tilde{h}_n \, \tilde{\phi}(2t - n) \tag{18}$$

In the same way, a duality wavelet is denoted by

$$\tilde{\psi}(t) = \sqrt{2} \sum_n \tilde{g}_n \, \tilde{\phi}(2t - n) \tag{19}$$

Finally, the duality scaling gives

$$\begin{cases} g_n = (-1)^n h_{(1-n)} \\ g_n = (-1)^n h_{(1-n)} \end{cases} \tag{20}$$

Biorthogonal Wavelet filter

Biorthogonal wavelet belongs to the family with compact supports example is bior. This is a powerful tool for image denoising. W. Sweldens pioneered the use of the lifting scheme (Uytterhoevenm et al., 1997) to create the biorthogonal wavelet. Lifting is a straightforward method for increasing the vanishing moments of duality wavelets. Cohen et al. and Swelden were the pioneers of the lifting system. The initial collection $g^0, \tilde{g}, h, \tilde{h}^0$ is presumptively believed as a term used to describe finite biorthogonal wavelets. As a result, a new package deal $g, \tilde{g}, h, \tilde{h}$ is gathered and made up of a finite biorthogonal filter.

$$\begin{cases} h(w) = h^0(w) + g(w)(s(2w)) \\ g(w) = g^0(w) + h(w)s2(w) \end{cases} \tag{21}$$

The scaling and duality wavelet filters are not altered, as can be seen from the above equations. As a result, biorthogonal functions are derived from the filters described above. The set package $\psi^0, \tilde{\psi}^0, \phi, \tilde{\phi}^0$ the biorthogonal scaling function is contained in the initial package set. Therefore, a new set package as $\psi, \tilde{\psi}, \phi, \tilde{\phi}$ is arrived.

$$\begin{cases} \psi(x) = \psi^0(x) - \sum_k S_k \phi(x-k) \\ \bar{\phi}(x) = 2 \sum_k \tilde{h}_k^0 \phi(2x-k) + \sum_k S_{(-k)} \tilde{\psi}(x-k) \\ \psi(x) = 2 \sum_k \tilde{g}_k \tilde{\phi}(2x-k) \end{cases} \tag{22}$$

S_k can be chosen at random in this case. The dual functions and wavelets derived from a simple scale function are manipulated by the value of S in this case.

b. Orthogonal

Properties: asymmetric, orthogonal, biorthogonal.

Wavelet transform is used to compress and split details into long, vertical and diagonal. The estimated image includes the pixel values, along with the general context details. If the image details are minimal, then reduce the threshold to 0. It will be fully undistorted if the energy stored is 100%. However, if some change in value is discovered, that signifies a loss of compression. In order to reach this equilibrium, the Haar wavelet is a perfect and noiseless solution for this problem.

Averaging and differentiation of the image matrix result in a sparse matrix that is highly compressible. It works well for image compression.

Figure 8. Wavelet and scaling functions of Haar

Scaling function ϕ wavalet function ψ
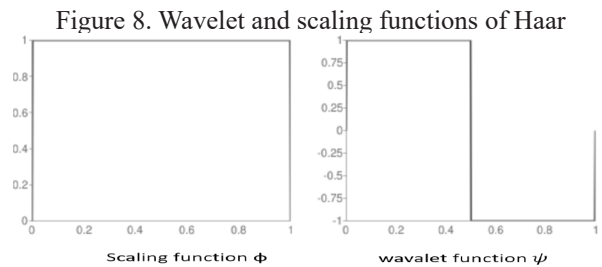
To obtain a new resolution with new pixel values, the first pairwise combination is computed. During this process, information is lost.

$$h_k(t) = \frac{1}{\sqrt{N}} \begin{cases} 2^{p/2} & (q-1)/2^p \le t < (q-0.5)/2^p \\ -2^{p/2} & (q-0.5)/2^p \le t < q/2^p \\ 0 & otherwise \end{cases} \tag{23}$$

The translation and dilation of the scaling function $\{\phi_{j,k}(x)\}$ composes the basis for V_j and W_j from $\{\psi_{j,k}(x)\}$. If they are orthonormal to each other, then it follows the below property:

$$\begin{cases} V_j \perp W_j \\ \langle \phi_{j,l}, \phi_{j,l'} \rangle = \delta_{j,l'} \langle \psi_{j,l}, \psi_{j,l'} \rangle = \delta_{j,l'} \\ \langle \phi_{j,l}, \psi_{j,l'} \rangle = 0 \end{cases} \quad (24)$$

c. Biorthogonal Wavelet

Properties: symmetric, not orthogonal, biorthogonal.

In signal and image reconstruction, linearity is a critical and advantageous feature. The freedom provided by a biorthogonal wavelet is greater than that of an orthogonal wavelet. Biorthogonal wavelets and a filter with a finite impulse response help exact and symmetrical reconstruction. We create a reverse biorthogonal wavelet by combining two biorthogonal wavelets. The biorthogonal wavelet graph is shown in Fig 9. The freedom provided by a biorthogonal wavelet is greater than that of an orthogonal wavelet. Biorthogonal wavelets and a filter with a finite impulse response help exact and symmetrical reconstruction.
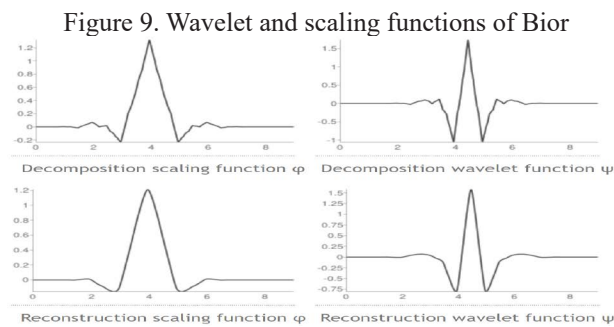
Figure 9. Wavelet and scaling functions of Bior

A biorthogonal wavelet proves two multiresolution analyses: $V_j, W_j, \phi_{j,k}, \psi_{j,k}$ and $\tilde{V}_j, \tilde{W}_j, \tilde{\phi}_{j,k}, \tilde{\psi}_{j,k}$. Dilation and translation of scaling function, $(\tilde{\phi}_{j,k}(x))$ and $(\tilde{\psi}_{j,k}(x))$, comprise the basis for $\tilde{V}_j$ and $\tilde{W}_j$ respectively. The biorthogonality satisfies the following properties:

$$\begin{cases} \tilde{V}_j \perp W_j \\ V_j \perp \tilde{W}_j \\ \langle \tilde{\phi}_{j,l}, \phi_{j,l'} \rangle = \delta_{l,l'} \\ \langle \tilde{\psi}_{j,l}, \psi_{j,l'} \rangle = \delta_{j,j'} \delta_{l,l'} \\ \langle \tilde{\phi}_{j,l}, \psi_{j,l'} \rangle = 0 \; and \; \langle \tilde{\psi}_{j,l}, \phi_{j,l'} \rangle = 0 \end{cases} \quad (25)$$

ALGORITHM: WAVELET-BASED DENOISING OF IMAGES USING MATLAB

The Global Threshold selection is implemented using the MATLAB. The following command is chosen:

Use of when CMP(): Function used for denoising images and compression of 1D or 2D signals

Imgden = wdencmp('gbl_or_lvd', img, 'wvname', N, THR, SORH, KEEPAPP)
Where,
Img: input noisy image and imgden: Output denoised image
Gbl_or_lvd: Either used 'gbl' for single global threshold or 'lvd' for level-dependent threshold
wvname: Name of wavelet used
N: Number of decomposition levels
THR: Threshold level(s) [Single value for 'gbl' and 3xN matric for 'lvd'. Three rows each for horizontal, diagonal, and Vertical detailed coefficients and n number of columns, where N is decomposition levels.
SORH: 's' or 'h' corresponding to soft and hard thresholding respectively.
KEEPAPP: either 0 or 1. If 1 approximation coefficients cannot be thresholded otherwise they can be thresholded.
OR
Use of ddencmp() : Function used for finding default values for denoising image or compression for 1D or 2D signals
• Imgden =[THR, SORH, KEEPAPP] = ddencmp('den', 'wvname', img)
Where,
Img: Input noisy image
THR: Default global threshold level.
SORH: 's' or 'h' corresponding to soft and hard thresholding respectively.

KEEPAPP: either 0 or 1. If 1 approximation coefficients cannot be thresholded otherwise they can be thresholded.

ddencmp() computes threshold value based on 'Universal Threshold' Method of Donoh.

$$\left[\lambda_j = \sigma_j \sqrt{2\log(N_j)} \right] \tag{26}$$

The following measures are included in the performance assessment procedures:

1. Add additive uniform noise type to image
2. Select Wavelet Type
3. Select level of decomposition
4. Apply Thresholding technique
5. De-noise the image
6. Compute the Noisy-SNR
7. Compute the Dnoiseed-SNR

RESULTS AND DISCUSSION

The SNR values of synthesis by denoising and enhancing terahertz hidden security image with the corresponding information filters coefficients are also compared. Finally, in the proposed Matlab algorithm, a comparison of SNR values obtained using Symlet-4, and bior-4.4 wavelets for Gaussian and salt & pepper noise is shown figure 10 and 11

Biorthogonal wavelet filters produce one scaling function and wavelet for decomposition and another pair for reconstruction, while orthogonal wavelet filter banks generate a single scaling function and wavelet.

Our findings show that using symmetric extension improves the performance of orthogonal wavelets significantly. Furthermore, our research reveals that linear filters are critical for denoising and compression images edges problem that has previously gone unnoticed.

We also show that when biorthogonal and orthogonal wavelets have similar filter properties and use symmetric extension, they produce similar compression and denoising

performance. The biorthogonal wavelets show a slight performance advantage for low frequency images; however, this advantage is much smaller than previously published results and can be explained by wavelet properties that were not previously considered.

Figure 10. Wavelet biorthogonal filter on salt &pepper vs Gaussian noise
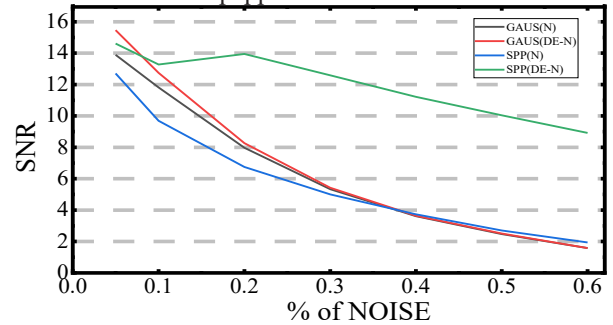
Figure 11. Wavelet Orthogonal filter on salt & pepper vs Gaussian noise
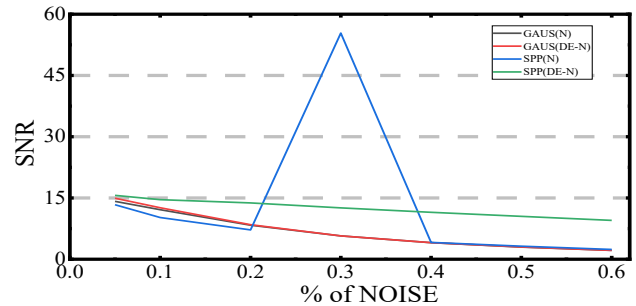
Figure 10 and 11, shows that whenever the percentage of the induced SNR noise type increases the denoised SNR wavelet filter which serves as a catalyst also varnishes along its horizontal, vertical, and diagonal detailed coefficient thresh. In figure 10 and 11 ,the green lines represents denoising at salt and pepper whiles red lines also indicates denoising at Gaussian. Biorthogonal bior4.4 and sym 4.0 for orthogonal is used in this work. Biorthogonal is the most effective in denoising filter for donoising salt and pepper noise as compared with denoising the Gaussian noise at the same percentage induced. It, therefore, makes wavelet localized feature in the image pixel data to have different scales as it preserves important image feature whiles removing noise from the image because wavelet denoising or wavelet

thresholding is the wavelet transform that leads to a sparse representation for images.

As Salt & pepper noise increases from 20% to 60%, the hidden security image as our target varnishes or over powered by the induced salt & pepper noise as shown in figure 13 and 15 though bior 4.4 and sym4.0 wavelet transform filters proves powerful in denoising the image but it still not clearer.

When an image is impaired by Gaussian noise, wavelet shrinkage denoising has been found to be nearly perfect in both bior4.4 and sym 4.0 than when the image is corrupted by salt & pepper noise. The visually comparative analysis of the Gaussian and salt & pepper noise parameters as shown in figures 12 to 15.

Figure 12. Using Biorthogonal bior4.4 filter @ Gaussian noise
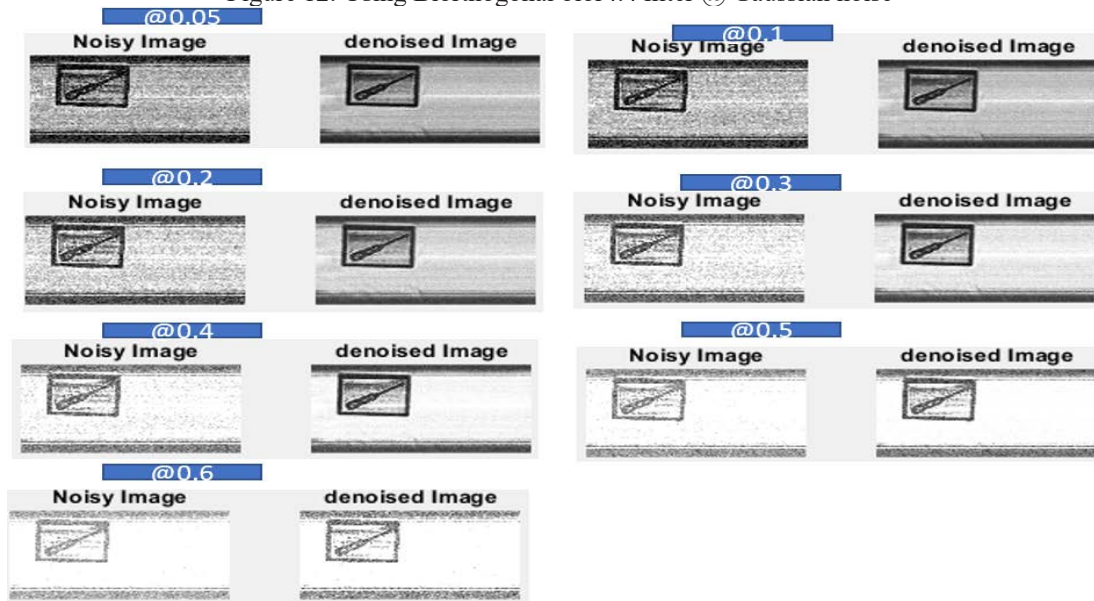
Figure 13. Using Biorthogonal bior4.4 filter @ Salt& pepper noise
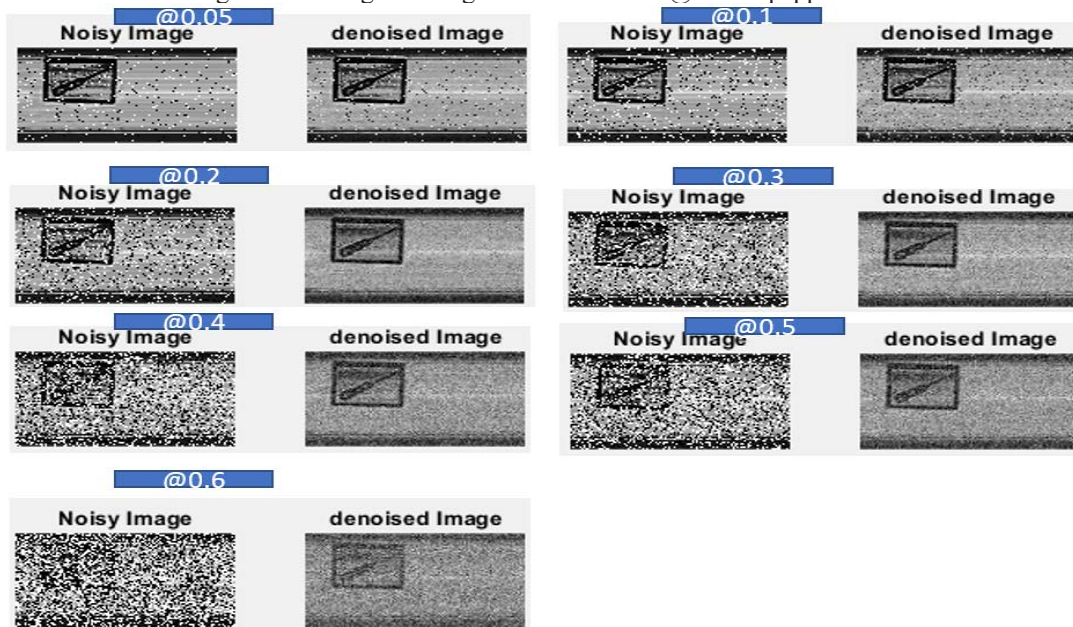
Figure 14. Using orthogonal sym4.0 filter @ Gaussian noise
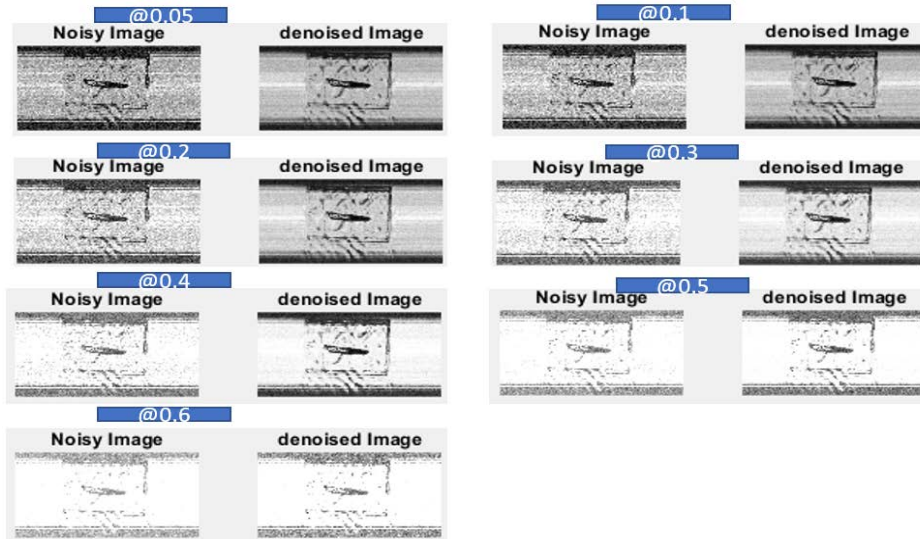
Figure 15. Using orthogonal sym4.0 filter @ Salt & pepper noise
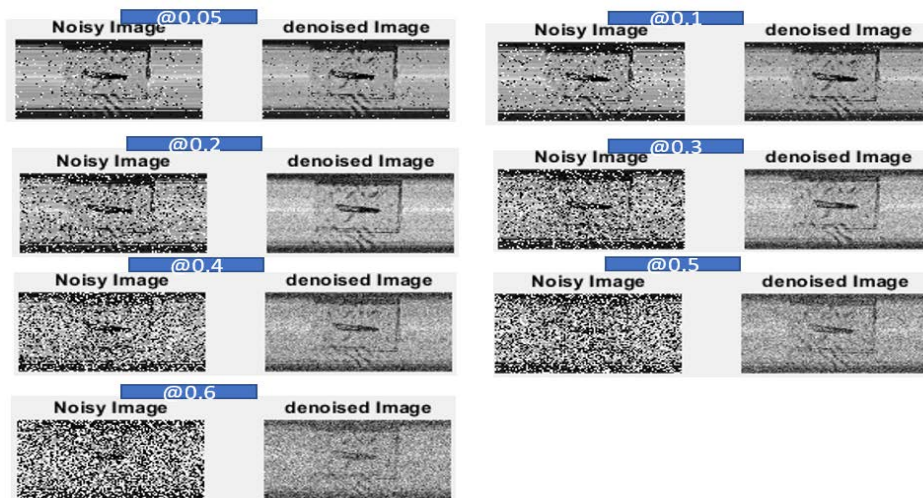
CONCLUSION

This work represents a comparison of denoising methods for Terahertz images both in the frequency domain filters. This outcome is a promising future for terahertz security application images. The frequency-domain denoising used in this work is the wavelet transform for high/low pass filters and low/high pass filters. It shows that biorthogonal filters are very effective to terahertz low resolution image due to some level of noise in the image whilst capturing process and after the transferring of images unto the disks. Since wavelets cannot simultaneously possess the desirable properties of orthogonality and symmetry, they are used for image denoising and enhancement. Biorthogonal wavelets have been the de facto norm for image denoising and compression applications for images, for a long time, their qualities contribute to image enhancement. The primary explanation for their superior success is the feasibility of symmetric extension with biorthogonal wavelets.

REFERENCES

Baili, J., Lahouar, S., Hergli, M., Al-Qadi, I. L., & Besbes, K. (2009). GPR signal de-noising by discrete wavelet transform. Ndt & E International, 42(8), 696-703. https://doi.org/10.1016/j.ndteint.2009.06.003

Boix, M., & Cantó, B. (2013). Using wavelet denoising and mathematical morphology in the segmentation technique applied to blood cells images. Mathematical Biosciences & Engineering, 10(2), 279. https://doi.org/10.3934/mbe.2013.10.279

Cheng, W., & Hirakawa, K. (2015). Minimum risk wavelet shrinkage operator for Poisson image denoising. IEEE Transactions on Image Processing, 24(5), 1660-1671. https://doi.org/10.1109/TIP.2015.2409566

Ercelebi, E. (2004). Electrocardiogram signals de-noising using lifting-based discrete wavelet transform. Computers in Biology and Medicine, 34(6), 479-493. https://doi.org/10.1016/s0010-4825(03)00090-8

Frost, V. S., Stiles, J. A., Shanmugan, K. S., & Holtzman, J. C. (1982). A model for radar images and its application to adaptive digital filtering of multiplicative noise. IEEE Transactions on pattern analysis and machine intelligence, (2), 157-166. https://doi.org/10.1109/tpami.1982.4767223

Gonzalez-Lee, M., Vazquez-Leal, H., Morales-Mendoza, L. J., Nakano-Miyatake, M., Perez-Meana, H., & Laguna-Camacho, J. R. (2021). Statistical assessment of discrimination capabilities of a fractional calculus based image watermarking system for Gaussian watermarks. Entropy, 23(2), 255. https://doi.org/10.3390/e23020255

Howlader, T., & Chaubey, Y. P. (2010). Noise reduction of cDNA microarray images using complex wavelets. IEEE transactions on Image Processing, 19(8), 1953-1967. https://doi.org/10.1109/TIP.2010.2045691

Jang, S. J., & Hwang, Y. (2020). Noise-aware and light-weight VLSI design of bilateral filter for robust and fast image denoising in mobile systems. Sensors, 20(17), 4722. https://doi.org/10.3390/s20174722

Jiang, Q. (2008). Compactly Supported Orthogonal and Biorthogonal $\sqrt 5$-Refinement Wavelets With 4-Fold Symmetry. IEEE transactions on image processing, 17(11), 2053-2062. https://doi.org/10.1109/TIP.2008.2004613

Laine, A. F. (2000). Wavelets in temporal and spatial processing of biomedical images. annual review of biomedical engineering, 2(1), 511-550. https://doi.org/10.1146/annurev.bioeng.2.1.511

Liu, X., Cheung, G., Ji, X., Zhao, D., & Gao, W. (2018). Graph-based joint dequantization and contrast enhancement of poorly lit JPEG images. IEEE Transactions on Image Processing, 28(3), 1205-1219. https://doi.org/10.1109/TIP.2018.2872871

Mallat, S. (1999). A wavelet tour of signal processing. Elsevier.

Mallat, S.G.(2009). A wavelet tour of signal processing. The sparse way, 3rd edn. Elsevier/Academic Press, Amsterdam, Boston.

Mishra, C., Samantaray, A. K., & Chakraborty, G. (2017). Rolling element bearing fault diagnosis under slow speed operation using wavelet de-noising. Measurement, 103, 77-86. https://doi.org/10.1016/j.measurement.2017.02.033

Naveed, K., Ehsan, S., McDonald-Maier, K. D., & Ur Rehman, N. (2019). A multiscale denoising framework using detection theory with application to images from CMOS/CCD sensors. Sensors, 19(1), 206. https://doi.org/10.3390/s19010206

Robinson, M. D., Toth, C. A., Lo, J. Y., & Farsiu, S. (2010). Efficient Fourier-wavelet super-resolution. IEEE Transactions on Image Processing, 19(10), 2669-2681. https://doi.org/10.1109/TIP.2010.2050107

Šesták, J., Planeta, J., & Kahle, V. (2020). Compact optical detector utilizing light emitting diodes, 50 nL L-shaped silica capillary cell and CCD spectrometer for simultaneous multi-wavelength monitoring of absorbance and fluorescence in microcolumn liquid chromatography. Analytica Chimica Acta, 1112, 80-91. https://doi.org/10.1016/j.aca.2020.03.020

Starck, J. L., Murtagh, F., & Fadili, J. M. (2010). Sparse image and signal processing: wavelets, curvelets, morphological diversity. Cambridge university press.

Terasense. (2020). Terasense_THz_Oscillator_(IMPATT_diode). www.terasense.com.

Uytterhoeven, G., Roose, D., Bultheel, A. (1997). Wavelet Transforms Using the Lifting Scheme.

Wang, X., Yin, L., Gao, M., Wang, Z., Shen, J., & Zou, G. (2019). Denoising method for passive photon

counting images based on block-matching 3D filter and non-subsampled contourlet transform. Sensors, 19(11), 2462. https://doi.org/10.3390/s19112462

Woods, Rafael C Gonzalez; Richard E. (2021). Digital Image Processing. https://www.biblio.com/digital-image-processing-by-woods-rafael-c-gonzalez/work/13949

Yang, M., Wang, F., Wang, Y., & Zheng, N. (2017). A denoising method for randomly clustered noise in ICCD sensing images based on hypergraph cut and down sampling. Sensors, 17(12), 2778. https://doi.org/10.3390/s17122778

Zhong, J., & Ning, R. (2005). Image denoising based on wavelets and multifractals for singularity detection. IEEE Transactions on Image Processing, 14(10), 1435-1447.https://doi.org/10.1109/tip.2005.849313